**Astronomy
&
Astrophysics**

Eclipse of the B3V companion and flaring of emission lines in V838 Monocerotis[*],[**]

U. Munari[1], R. L. M. Corradi[2,3], A. Henden[4], H. Navasardyan[1], M. Valentini[1], R. Greimel[2], P. Leisy[2,3], T. Augusteijn[5],
A. A. Djupvik[5], L. Glowienka[5], A. Somero[5], I. G. de la Rosa[3], A. Vazdekis[3], I. Kolka[6], and T. Liimets[6]

[1] INAF – Osservatorio Astronomico di Padova, via dell'Osservatorio 8, 36012 Asiago (VI), Italy
    e-mail: ulisse.munari@oapd.inaf.it
[2] Isaac Newton Group of Telescopes, Apartado de Correos 321, 38700 Sta. Cruz de La Palma, Spain
[3] Instituto de Astrofísica de Canarias, 38205 La Laguna, Tenerife, Spain
[4] American Association of Variable Star Observers, 49 Bay State Road, Cambridge, MA 02138, USA
[5] Nordic Optical Telescope, Apartado de Correos 474, 38700 Sta. Cruz de La Palma, Spain
[6] Tartu Observatory, Toravere 61602, Estonia

ABSTRACT

After four years during which only the spectacular light echo was showing continuous and rapid evolution while the central star was nearly constant, in autumn 2006 V838 Mon began a sequence of events which profoundly altered its spectroscopic and photometric behavior: (*a*) an eclipse of the B3V companion, characterized by the disappearance and reappearance of the B3V companion from optical spectra, and an eclipse-like lightcurve of ~70 day duration and $\Delta B \sim 1.15$ mag, $\Delta V \sim 0.55$ mag, $\Delta R_C \sim 0.10$ mag maximum depth; (*b*) a large increase in intensity of the [FeII] and FeII emission lines, and the appearance in emission for the first time since the 2002 outburst of Hα and higher Balmer series lines. While the [FeII] and FeII lines maintained a very sharp and unresolved profile, the Hα developed into a wide and structured profile, characterized by a sharp central reversal at the same velocity as one of the CO radio emission components. The disappearance of the B3V companion is equally well explained by a grazing eclipse from the outbursting L-type supergiant or by an eclipse from a dust cloud characterized by $E_{B-V} = 0.55$ and $R_V = 3.1$. We believe the flaring of the emission lines occurred at a similar time as the B3V eclipse just by chance.

Key words. stars: individual: V838 Monocerotis – stars: winds, outflows – stars: emission-line, Be – binaries: eclipsing

1. Introduction

V838 Mon is no doubt one of the most fascinating and studied individual objects of the last few years. Discovered in outburst on January 6, 2002 (Brown 2002), it soon attracted interest for its spectrum characterized by a cool, extended, optically thick and expanding atmosphere, with a complex pattern of metallic lines in absorption, some displaying P-Cyg profiles of several hundred km s^{-1} terminal velocity (Munari et al. 2002). The much brighter second maximum reached in early February changed the spectral appearance to that of an early A-type giant with a large flare-up of hydrogen emission lines, while ionized metals with P-Cyg profiles replaced neutral ones. Shortly after that, we discovered the emergence of a light echo around V838 Mon, the first in several decades in the Galaxy (Henden et al. 2002). The light echo progressively increased in size and brightness to become easily observable even with backyard telescopes, while the Hubble Space Telescope started following, and it is still tracking, the details of its spectacular evolution (Bond et al. 2003, 2007).

At the beginning of April 2002, V838 Mon went through a rapid drop in optical brightness ($\Delta B = 6.5$ mag) caused by a rapid cooling of the photospheric temperature that, in just one month, caused the spectra to sweep through the entire sequence of M giant spectral types and beyond, venturing into the temperature regime of L-type brown dwarfs while retaining supergiant dimensions. Balmer and all other emission lines switched off and minimum surface temperature was reached around January 2003, when the radius was $R \sim 6000\ R_\odot$ and $T_{\rm eff} \sim 2000$ K (Pavlenko et al. 2007). At the same time, the surface cooling (and thus shifting of the emission peak of the outbursting component to the IR) allowed the discovery at U and B wavelengths of a B3V companion (Desidera & Munari 2002). Since January 2003 the outbursting component has entered a very slow and monotonic increase in photospheric temperature so that its optical colors and molecular spectrum in mid-2006 resembled those of the coolest known M-type super-giants.

A recent conference was devoted entirely to V838 Mon (Corradi & Munari 2007), with detailed reviews of the photometric (Henden 2007) and spectroscopic evolution (Munari et al. 2007) until summer 2006. In this paper we report the large and completely unanticipated photometric and spectroscopic changes that occurred in V838 Mon at the end of 2006, after four years of remarkable stability and that add further complexity to this intriguing and extremely peculiar object. It deserves continuous monitoring at all wavelengths given its inclination to offer continued surprises to its devoted observers.

---

[*] Tables 2–4 are only available in electronic form at
http://www.aanda.org

[**] Based on observations made with the Asiago 1.82 m of the INAF Astronomical Observatory of Padova, and with 4.2 m WHT and 2.5 m INT operated by the Isaac Newton Group of Telescopes, and with the 2.6 m NOT operated jointly by Denmark, Finland, Iceland, Norway, and Sweden, in the Spanish Observatorio del Roque de Los Muchachos of the Instituto de Astrofísica de Canarias.

There are at least two other known objects with spectroscopic and photometric evolution very similar to that of V838 Mon. M 31-RV (Rich et al. 1989; Mould et al. 1990; Boschi & Munari 2004) erupted in the bulge of the Andromeda Galaxy (M 31) in 1988, developed an M-type supergiant spectrum at optical maximum with pronounced P-Cyg profiles and Balmer lines in emission, and peaked to $M_V = -9.95$. V4332 Sgr (Martini et al. 1999; Munari et al. 2007) erupted in 1994 in the Bulge of our galaxy, peaked at $M_{Rc} \sim -9$, and it too developed at optical maximum an M-type supergiant spectrum with Balmer and FeII + [FeII] emission lines. For both M 31-RV and V4332 Sgr, the observations stopped at the time when the objects were rapidly sweeping through the M-type supergiant spectral sequence (cf. Munari et al. 2007, their Fig. 8), so it is not known if they too ended up developing an L-type supergiant spectrum.

Kimeswenger (2007) has proposed that V1148 Sgr could also be related to V838 Mon type of objects. Discovered as Nova Sgr 1943, it was observed by Mayall (1949) to develop K- and M-type absorption spectra. Not much else is known about this object. Kulkarni et al. (2007) has recently described a bright optical transient source (named M 85 OT2006-1) which appeared in early 2006 in the lenticular galaxy M 85 in the Virgo cluster. It peaked at $M_{Rc} \sim -12$, and developed Balmer emission lines on top of a cool spectral energy distribution ($T_{eff} \approx 4600$ K). The analogy with V838 Mon is probably even deeper. In fact, looking in detail at Fig. 3 of Kulkarni et al. (2007) which zooms onto a small portion around Hα of their Keck LRIS spectrum for February 24.59, 2006 UT, a deep and wide P-Cyg line profile appears at the (red-shifted) position of BaII 6497 Å. BaII lines displayed spectacular P-Cyg profiles in V838 Mon too (cf. Fig. 4 of Munari et al. 2007), especially at the time its continuum mimicked an early K-type supergiant of a temperature similar to that derived by Kulkarni et al. (2007) for M 85 OT2006-1. Kato (2003) discussed CK Vul, which erupted in 1670, in relation to V838 Mon. The association with V838 Mon however could be spurious according to van Hoof et al. (2006) and Kimeswenger (2007), who both prefer a late or very late thermal pulse interpretation for this object. A detailed, multi-frequency investigation by Hajduk et al. (2007) highlights a complex structure in CK Vul revealing at its center what seems to be the remnant of a circumbinary disk, as seen in some binary post-AGB stars.

A wide range of possible explanations have been offered to account for V838 Mon-type eruptions. Iben & Tutukov (1992) modeled M31-RV in terms of a cool WD accreting at a very low rate from a companion, and under such circumstances the *entire* WD should have experienced a thermonuclear runaway. To account for V838 Mon, Soaker & Tylenda (2003, see also Tylenda & Soker 2006) proposed a stellar merger in a 8 + 0.3 $M_\odot$ binary system, while Retter & Marom (2003, see also Retter et al. 2006) opted for an expanding giant which swallowed orbiting planets. Lawlor (2005, 2007) discussed a model for the outburst of V838 Mon based on a born-again plus accretion scenario on a 1 $M_\odot$ star in a binary system. Munari et al. (2005) suggested for V838 Mon a helium flash on a once more massive progenitor, evolved by heavy mass-loss into the region of Wolf-Rayet stars at the time of observed eruption. Goranskij et al. (2007) similarly argued in favor of a hot and massive progenitor binary system for V4332 Sgr.

2. Observations

CCD photometry has been obtained with the Sonoita Research Observatory 0.35-m robotic telescope, using BVR_CI_C filters and an SBIG STL-1001E CCD camera. Pixel size is 1.25″/pix and
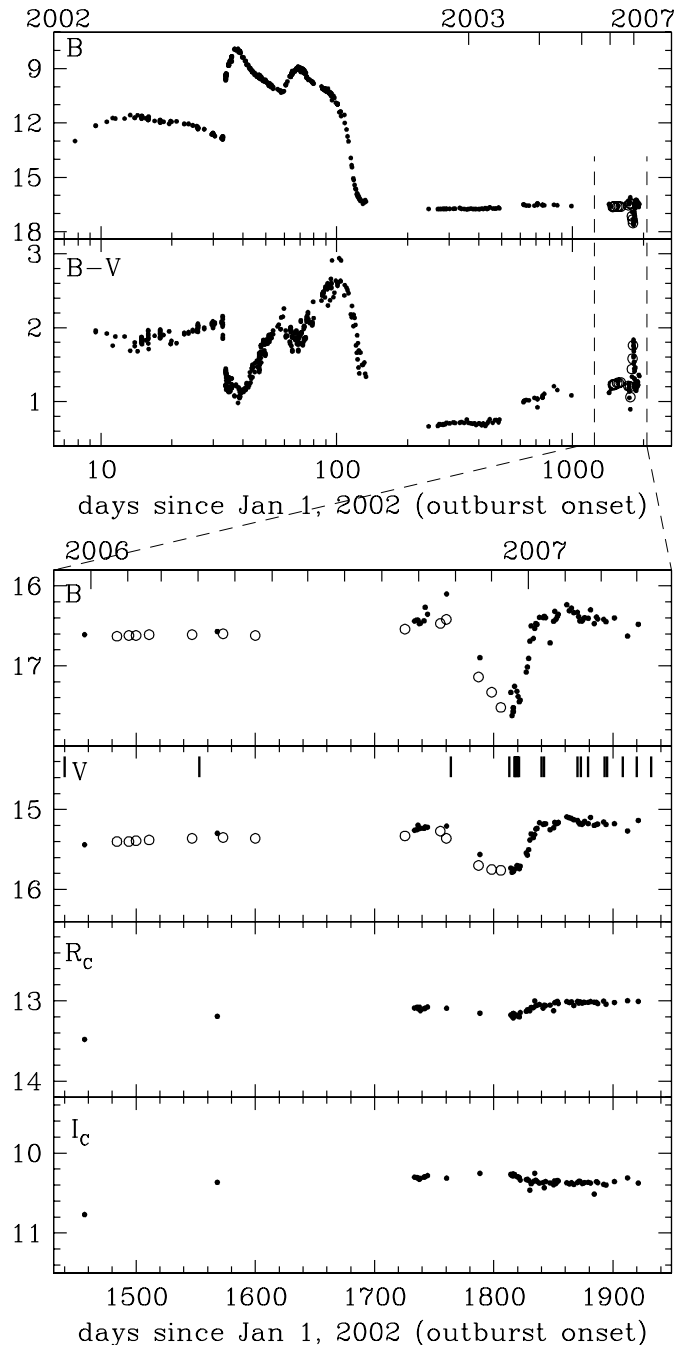
Fig. 1. *Upper panels*: B and $B-V$ evolution of V838 Mon since outburst onset (data from Henden 2007 and Table 2). *Lower panels*: zooming on the evolution during the last 16 months. The vertical bars on the V panel mark the epochs of the spectra listed in Table 1. The filled circles are our observations from Table 2, open circles represent observations by Goranskij (2006) and Bond (2006).

the field of view is $20 \times 20'$. Exposure times were 8×300 s in B, 4×240 s in V, 4×120 s in R_C and 4×60 s in I_C. PSF fitting was adopted instead of aperture photometry, due to the proximity of similar-brightness companion stars. The photometric data are presented in Table 2 (available electronically only) and plotted in Fig. 1.

Spectroscopic observations of V838 Mon were obtained with a number of instruments and a journal of the observations is given in Table 1. Low and medium resolution, absolutely fluxed spectra of V838 Mon have been regularly secured since the

Table 1. Journal of our spectroscopic observations of V838 Mon.

date	range (Å)	disp. (Å/pix)	resol. (Å)	instrument
2006 Apr 02	3910 - 7793	4.25	10.5	Asiago 1.8m + AFOSC
	8269 - 9167	0.88	2.42	”
Oct 30	3948 - 5954	1.61	4.90	WHT + INTEGRAL
	6030 - 9128	1.61	5.10	”
Dec 18	3856 - 5544	0.44	1.70	WHT 4.2m + ISIS
22	3880 - 7796	4.25	10.5	Asiago 1.8m + AFOSC
	6348 - 7078	0.72	2.00	”
	8269 - 9167	0.88	2.42	”
23	6378 - 6682	0.26	0.65	NOT 2.6m + ALFOSC
24	6378 - 6682	0.26	0.65	”
25	6378 - 6682	0.26	0.65	”
26	3945 - 4723	0.22	0.75	WHT 4.2m + ISIS
	5862 - 6637	0.25	0.68	”
31	6378 - 6682	0.26	0.65	NOT 2.6m + ALFOSC
2007 Jan 14	6204 - 7248	0.47	0.98	INT 2.5m + IDS
16	6204 - 7248	0.47	0.98	”
Feb 13	3500 - 7800	4.25	10.5	Asiago 1.8m + AFOSC
	6348 - 7078	0.72	2.00	”
	8269 - 9167	0.88	2.42	”
16	3210 - 5190	1.93	4.25	Asiago 1.8m + AFOSC
22	6378 - 6682	0.26	0.65	NOT 2.6m + ALFOSC
Mar 10	3500 - 7800	4.25	10.5	Asiago 1.8m + AFOSC
	6348 - 7078	0.72	2.00	”
23	3210 - 5190	1.93	4.25	Asiago 1.8m + AFOSC
Apr 04	6378 - 6682	0.26	0.65	NOT 2.6m + ALFOSC
16	3210 - 5190	1.93	4.25	Asiago 1.8m + AFOSC
20	5000 - 7800	4.25	10.5	Asiago 1.8m + AFOSC

outburst in January 2002 with the AFOSC imager+spectrograph mounted on the 1.82 m telescope operated in Asiago by INAF Astronomical Observatory of Padova. Spectra of V838 Mon were collected also with several telescopes of the Observatorio del Roque de los Muchachos (La Palma, Spain).

3. Eclipse of the B3V companion

After four years of extremely quiet and flat behaviour (Fig. 1) suddenly, in late October 2006, V838 Mon began a steep decline in brightness which reached a minimum around mid-December and returned to normal brightness by early January 2007. The amplitude of the event was $\Delta B \sim 1.15$, $\Delta V \sim 0.55$, and $\Delta R_C \sim 0.10$ mag. We interpret the event as an eclipse of the B3V companion. In fact, during the eclipse the signatures of the B3V companion disappeared from the spectra, as clearly shown in Fig. 3, to reappear as soon as the system had regained normal brightness.

In Fig. 2, the spectrum for December 22, obtained close to minimum, shows deeper than usual molecular absorptions from the L-type supergiant (hereafter LtSG). In fact, such molecular absorptions reach zero intensity in their cores, and outside the eclipse they are partially filled-in by the emission from the B3V companion. The apparently deeper molecular absorptions in December do not trace photospheric changes in the LtSG but instead confirm the eclipse scenario and account well for the observed $\Delta R_C = 0.10$ mag depth. An early suggestion for an eclipse of the B3V companion was made by Goranskij (2006) in December 2006 on the basis of B-band photometry showing the initial declining portion of the photometric profile (Fig. 1 open circles).

To have witnessed an eclipse in V838 Mon is indeed a lucky coincidence, in line with the continued surprises with which V838 Mon delights its fellow observers. Its duration was about 70 days from start to ingress to end of egress, and could have gone undetected if it had occurred during summer conjunction with the Sun. It is also a quite rare event. None have been detected in the previous 5 years of close photometric monitoring (Fig. 1). What caused this eclipse? There are two equally viable explanations.

The first one sees a dust cloud, absorbing according to the standard $R_V = 3.1$ law, that passes in front of the B3V star alone, without affecting the LtSG component. A direct integration of the resulting combined spectra energy distribution shows that a reddening by $E_{B-V} = 0.55$ of the B3V would cause a drop in brightness of the combined binary system of $\Delta B \sim 1.15$, $\Delta V \sim 0.56$, and $\Delta R_C \sim 0.07$ mag, thus essentially identical to what observed. Such an eclipsing cloud should probably be gravitationally bound to the B3V+LtSG binary. Its origin is unclear, perhaps connected to blobs of material thrown away by the LtSG at the time of heaviest mass loss during early outburst phases.

A second possibility is an eclipse of the B3V star by the LtSG companion. If the Pavlenko et al. (2007) estimate of a peak radius of 6000 $R_\odot$ for the LtSG in winter 2002/03 is correct, the minimum orbital semi-major axis must be 6000 $R_\odot$ ($\equiv$28 AU) because at that time the B3V companion was still visible and therefore external to the LtSG outer radius. Adopting 7 $M_\odot$ for the main sequence B3V companion, the orbital period corresponding to the 28 AU lower limit to the orbital separation is 40 yr for an LtSG mass of 7 $M_\odot$, and 20 yr for 40 $M_\odot$[1]. The possibility of a heavy LtSG (progenitor) has been discussed by Munari et al. (2005) and Hirschi (2007). The eclipse lasted for $\leq 1/150$ of the orbital period, and in spite of the huge difference in radius of the two stars (B3V and LtSG) it did not go through a flat bottom. This means that the eclipse was a grazing one, by the outer layers of the LtSG atmosphere. A grazing eclipse in turn means that searching for past eclipses in photographic plate archive should *not* pay dividends. In fact, before the outburst, the radii of the two companion stars were similar according to photometry in quiescence (Goranskij et al. 2007). If we observe a grazing eclipse when the occulting body expanded by $\sim$100×, it is quite probable that in quiescence the B3V passed well clear of the companion at orbital prospective conjunctions.

4. Flaring of emission lines

Shortly before the eclipse events discussed in the previous section, in late September 2006, the strength of [FeII] and FeII emission lines began increasing in V838 Mon, while Hα turned into emission for the first time since the initial phases of the 2002 outburst. The last time Hα was seen in emission was in April 2002 (cf. Munari et al. 2007). Since the strongest [FeII] and FeII emission lines cluster between 4200 and 4600 Å, their increase in intensity caused the brightening in the B-band visible in Fig. 1 just before the onset of the eclipse fading. This had no counterpart in the V-band due to the lower concentration of

---

[1] Some authors preferred smaller maximum radii for the LtSG (e.g. Tylenda 2005). Two years after maximum expansion was reached, interferometric observations by Lane et al. (2005) gave an apparent radius of 0.92 mas, corresponding to a linear radius of 2000 $R_\odot$ for a distance of 10 kpc. A 2000 $R_\odot$ lower limit to the orbital separation would shorten the minimum orbital period to 7.5 and 4 yr for LtSG masses of 7 and 40 $M_\odot$, respectively.
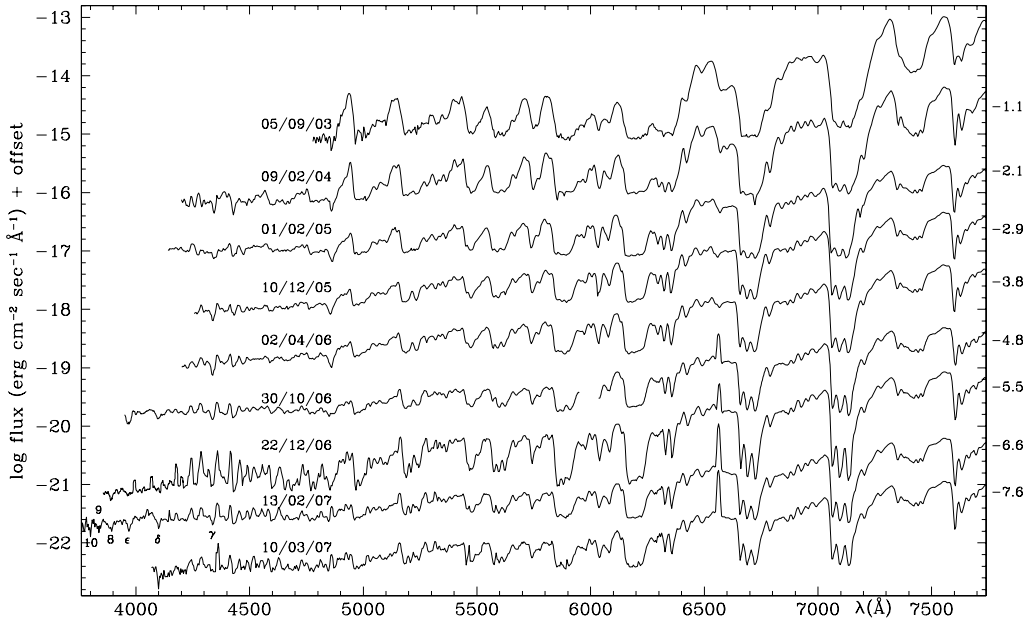
Fig. 2. Selection of Asiago 1.82 m + AFOSC spectra to highlight the general spectral evolution of V838 Mon during the last four years (cf. Munari et al. 2007). The spectra are on the same ordinate scale and are displaced for clarity by the log offsets listed to the right. The spectrum for Oct. 30, 2006 is from WHT (cf. Table 1), and has been degraded to the same resolution of the other Asiago spectra.
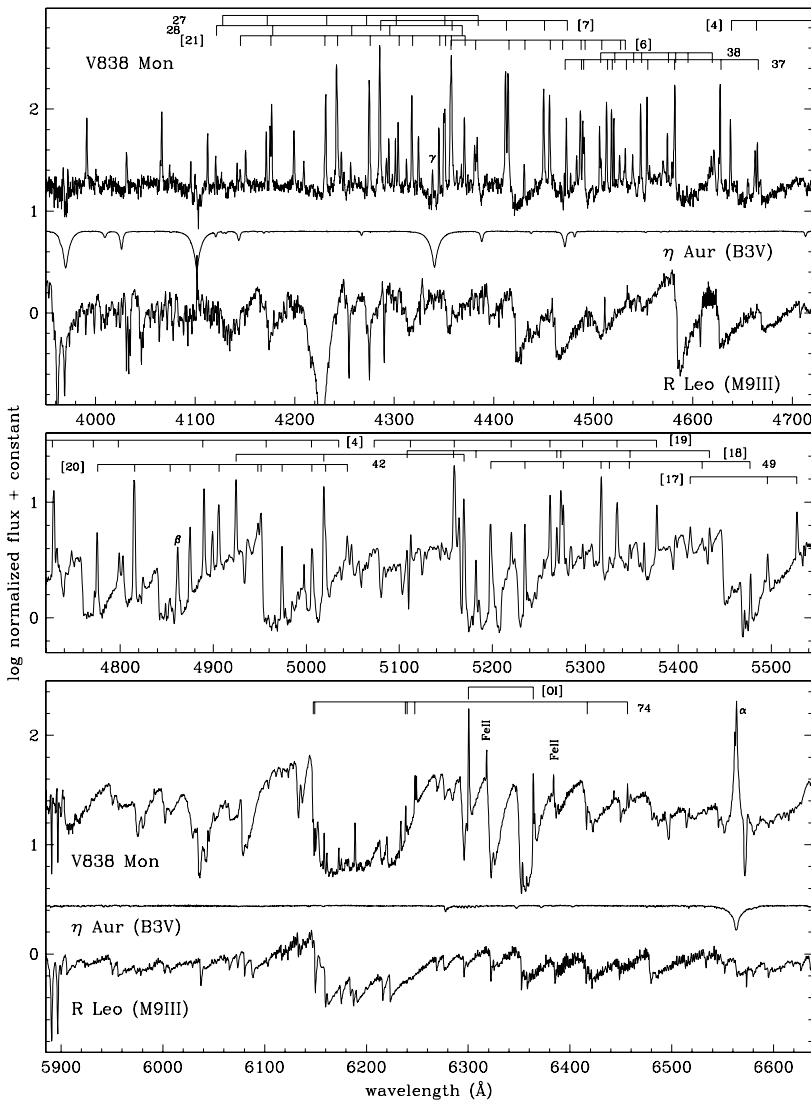
Fig. 3. The top and bottom panels show the WHT + ISIS spectrum of V838 Mon we obtained on December 26, 2006. The same night, and with an identical instrument set-up, we recorded for comparison the spectra of R Leo (M9III) and η Aur (B3V). The central panel fills in the wavelength gap in the December 26, 2006 spectra by showing the corresponding portion of a lower resolution WHT + ISIS spectrum of V838 Mon for December 18, 2006. The spectra are continuum normalized and their ordinate step is the same in all panels. Note the logarithmic scale of ordinates required by the huge intensity of the emission lines. The emission lines belonging to strongest FeII and [FeII] multiplets are identified by their numbers (Table 4).
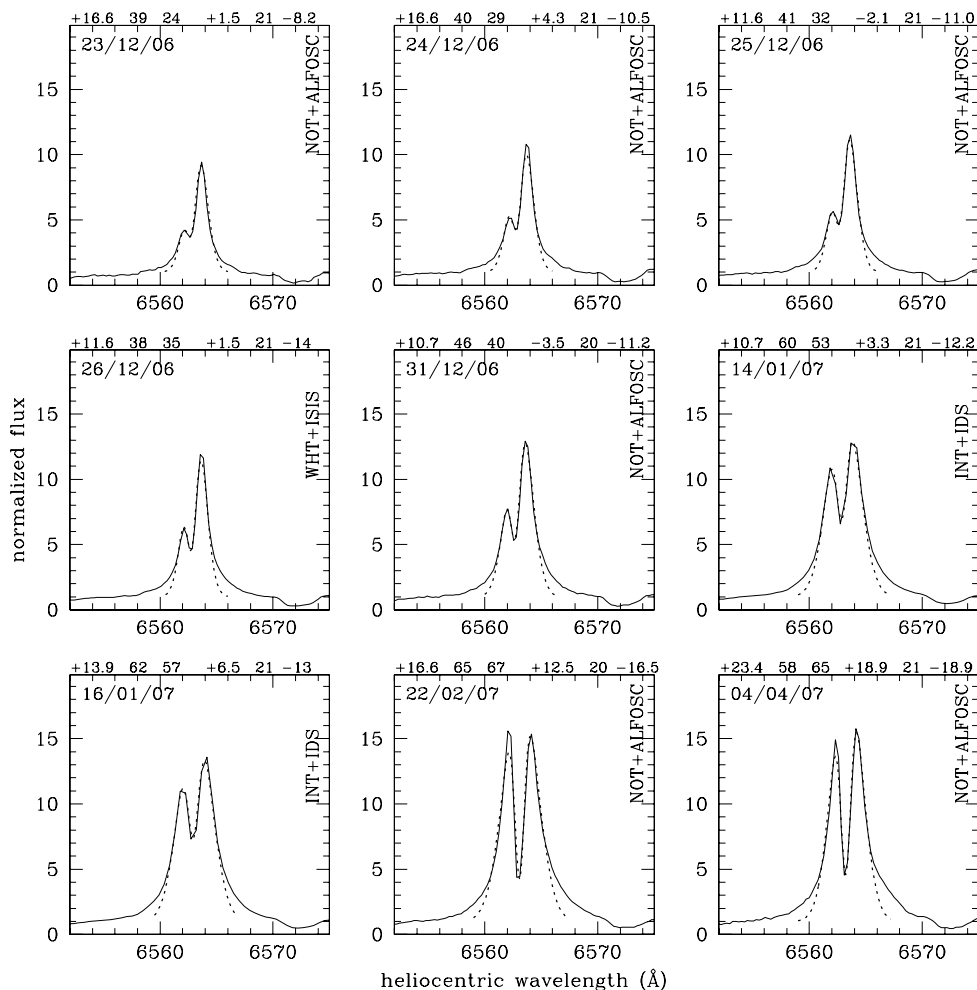
Fig. 4. Evolution of the Hα profile. Over-plotted is the fit (dotted line) with two Gaussians, one in emission and the other in absorption. The six numbers at the top of each panel represent the central heliocentric velocity (in km s^{-1}), the dispersion in velocity (in km s^{-1}) and the equivalent width (Å) of the emission and absorption fitting Gaussian, respectively. The acquisition in ToO mode for some of the spectra does not guarantee a strict control on the zero point of the wavelength scale.
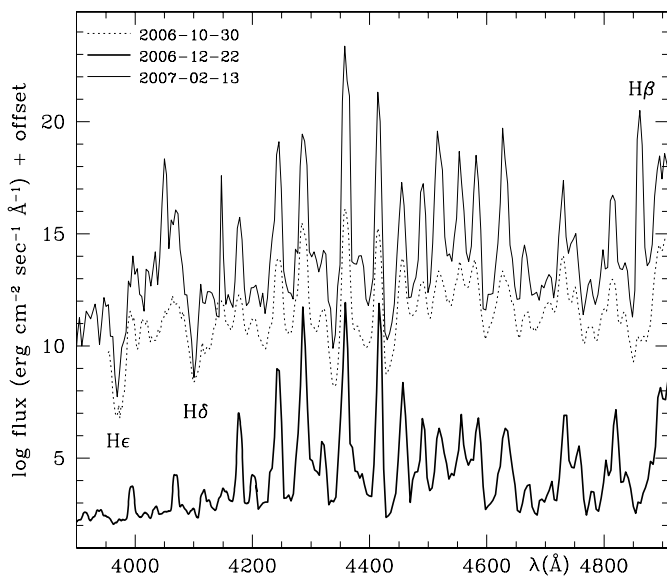
Fig. 5. Comparison of the blue portion of the V838 Mon spectra for October 30 and December 22, 2006 and February 13, 2007.

[FeII] and FeII emission lines and the much brighter background of the LtSG continuum, which steeply rises toward redder wavelengths. The fact that (*a*) the emission lines began their growth in intensity *before* the eclipse event took place, (*b*) the phenomenon smoothly continued *after* the eclipse-like phase was over; and (*c*)

the Hα profile evolution was not in phase with the eclipse event, suggests that the two events (eclipse and emission line flaring) were not related and appeared at similar times just by chance.

On the high resolution, high S/N WHT+ISIS spectra for December 18 and 26 (Fig. 3) we identified more than 200 emission lines. At that time, V838 Mon was going through the minimum of the eclipse, and the weaker continuum further increased the contrast of emission lines. The increase in the number of detected emission lines is ≥20× compared to published previous observations (e.g. Barsukova et al. 2007, observations covering 2004–2005). The radial velocity, integrated absolute flux and identification of the emission lines in our December 18 and 26 spectra, are given in Tables 3 and 4 (available electronic only). The vast majority of them belong to FeII (multiplets 20, 22, 27, 28, 32, 37, 38, 42, 43, 49, 54, 74) and [FeII] (multiplets 4, 6, 7, 17, 18, 19, 20, 21, 24, 35, 36), with forbidden lines much stronger than permitted ones. These lines are intrinsically sharp enough to be unresolved. The underlying continuum is highly structured because of the molecular absorption spectrum of the LtSG. This affects the accuracy of flux measurements, and in some cases can mimic the presence of P-Cyg absorptions. However, when the lines of the same multiplet are compared in velocity space, it is clear that FeII emission lines do *not* display absorption components.

Figure 4 displays the large evolution in intensity and shape of the Hα emission profile from December 23, 2006, to April 4, 2007. The profile is characterized by a sharp central reversal. We have fitted the Hα profiles with two Gaussians, a broader

one in emission and a sharper one in absorption, and the results are given in Fig. 4. The sharp absorption component has kept a very stable velocity dispersion of 20.5 km s^{-1} and has increased its equivalent width by 2.3 times (from 8.2 to 18.9 Å), while the emission component has smoothly increased its velocity dispersion from 40 to 60 km s^{-1} and its equivalent width by 2.7 times (from 24 to 65 Å). The relative velocity of the emission component with respect to absorption has been declining from +13.5 to +4.3 km s^{-1}. Even if similarly double-peaked, the Hα profiles seem quite different from those originating from accretion disks, both optically thin and thick, of the type seen in interacting binaries (e.g. Horne & Marsh 1986).

Detailed modeling of FeII, [FeII] emission line spectrum is a complex and not yet fully understood process (e.g. Viotti et al. 1999), far beyond the scope of this paper, and it will be discussed elsewhere together with modeling of the Hα profile evolution. However, it is intriguing to note that the velocity of the absorption component ($\langle RV_{\odot}^{\mathrm{abs}} \rangle = +4.8$ km s^{-1} corresponding to $\langle RV_{\mathrm{LSR}}^{\mathrm{abs}} \rangle = -12.5$ in the Local Standard of Rest) is within 2 km s^{-1} of the $V_{\mathrm{LSR}} = -11$ km s^{-1} of the CO radio emission detected in V838 Mon for the first time in December 2005 by Kaminski et al. (2007). The velocity of the Hα emission component ($\langle RV_{\odot}^{\mathrm{ems}} \rangle = +14.6$ km s^{-1} $\equiv$ $\langle RV_{\mathrm{LSR}}^{\mathrm{ems}} \rangle = -2.8$) is the same as that of FeII, [FeII] ($\langle RV_{\odot} \rangle = +15.3$ km s^{-1} $\equiv$ $\langle RV_{\mathrm{LSR}} \rangle = -2.1$ km s^{-1}) and is not related to the other component seen in CO at $V_{\mathrm{LSR}} = +53.4$ km s^{-1} by Kaminski et al. (2007) or in the SiO maser at $V_{\mathrm{LSR}} = +54.3$ km s^{-1} by Deguchi et al. (2007).

References

Barsukova, E. A., Goranskij, V. P., Abolmasov, P. K., Fabrika, S. N., et al. 2007, in The Nature of V838 Mon and Its Light Echo, ed. R. L. M. Corradi, & U. Munari, ASP Conf. Ser., 363, 206

Bond, H., 2006, ATel, 966

Bond, H. 2007, in The Nature of V838 Mon and Its Light Echo, ed. R. L. M. Corradi, & U. Munari, ASP Conf. Ser., 363, 130

Bond, H., Henden, A., Leavy, Z. G. et al. 2003, Nature, 422, 405

Boschi, F., & Munari, U. 2004, A&A, 418, 869

Brown, N. J. 2002, IAUC, 7785

Corradi, R. L. M., & Munari, U. 2007, ed. The Nature of V838 Mon and Its Light Echo, ASP Conf. Ser., 363

Desidera, S., & Munari, U. 2002, IAUC, 7982

Deguchi, S., Matsunaga, N., & Fukushi, H. 2007, in The Nature of V838 Mon and Its Light Echo, ed. R. L. M. Corradi, & U. Munari, ASP Conf. Ser., 363, 81

Goranskij, V. 2006, ATel, 964

Goranskij, V., Metlova, N. V., Shugarov, S. Yu., et al. 2007, in The Nature of V838 Mon and Its Light Echo, ed. R. L. M. Corradi, & U. Munari, ASP Conf. Ser., 363, 214

Hajduk, M., Zijlstra, A. A., van Hoof, P. A. M., et al. 2007, MNRAS, 378, 1298

Henden, A. 2007, in The Nature of V838 Mon and Its Light Echo, ed. R. L. M. Corradi, & U. Munari, ASP Conf. Ser., 363, 3

Henden, A., Munari, U., & Schwartz, M. 2002, IAUC, 7859

Hirschi, R. 2007, in The Nature of V838 Mon and Its Light Echo, ed. R. L. M. Corradi, & U. Munari, ASP Conf. Ser., 363, 257

Horne, K., & Marsh, T. R. 1986, MNRAS, 218, 761

Iben, I. Jr., & Tutukov, A. V. 1992, ApJ, 389, 369

Kaminski, T., et al. 2007, in The Nature of V838 Mon and Its Light Echo, ed. R. L. M. Corradi, & U. Munari, ASP Conf. Ser., 363, 103

Kato, T., Miller, M., Szczerba, R., Tylenda, R. 2003, A&A, 399, 695

Kimeswenger, S. 2007, in The Nature of V838 Mon and Its Light Echo, ed. R. L. M. Corradi, & U. Munari, ASP Conf. Ser., 363, 197

Kulkarni, S. R., Ofek, E. O., Rau, A., et al. 2007, Nature, 447, 458

Lane, B. F., Retter, A., Thompson, R. R., Eisner, J. A., et al. 2005, ApJ, 622, L137

Lawlor, T. M. 2005, MNRAS, 361, 695

Lawlor, T. M. 2007, in The Nature of V838 Mon and Its Light Echo, ed. R. L. M. Corradi, & U. Munari, ASP Conf. Ser., 363, 249

Martini, P., Wagner, R. M., Tomaney, A., et al. 1999, AJ, 118, 1034

Mayall, M. W. 1949, AJ, 54, R191

Mould, J., Cohen, J., Graham, J. R., et al. 1990, ApJ, 353, L35

Munari U., Henden A., Kiyota S., et al. 2002, A&A, 389, L51

Munari, U., Henden, A., Vallenari, A., et al. 2005, A&A 434, 1107

Munari, U., Navasardyan, H., Villanova, S., et al. 2007, in The Nature of V838 Mon and Its Light Echo, ed. R. L. M. Corradi, & U. Munari, ASP Conf. Ser., 363, 13

Pavlenko, Ya. V., Kaminsky, B., Lyubchik, Y., Yakovina, L., et al. 2007, in The Nature of V838 Mon and Its Light Echo, ed. R. L. M. Corradi, & U. Munari, ASP Conf. Ser., 363, 225

Retter, A., & Marom, A. 2003, MNRAS, 345, L25

Retter, A., Zhang, B., Siess, L., & Levinson, A. 2006, MNRAS, 370, 1573

Rich, R. M., Mould, J., Picard, A., et al. 1989, ApJ, 341, L51

Soaker, N., & Tylenda, R. 2003, ApJ, 582, L105

Tylenda, R. 2005, A&A, 436, 1009

Tylenda, R. 2006, A&A, 451, 223

Tylenda, R., & Soker, N. 2006, A&A, 451, 223

van Hoof, P. A. M., Bryce, M., Evans, A., et al. 2006, in Planetary Nebulae in our Galaxy and Beyond, ed. M. J. Barlow, & R. H. Mendez, IAU Symp., 234, 75

Viotti, R., Rossi, C., Baratta, G. B., et al. 1999, in ASP Conf. Ser., 179, 184

Online Material

Table 2. Our CCD photometry of V838 Mon since October 2006. HJD is the heliocentric JD − 2450000.

HJD	V	$B - V$	$V - R_C$	$R_C - I_C$
53704.8042	15.347 ±0.007	1.122 ±0.029	2.084 ±0.009	2.799 ±0.010
53704.8046	15.380 ±0.009	1.117 ±0.031	2.103 ±0.009	2.823 ±0.007
53842.6436	15.296 ±0.008	1.275 ±0.019	2.103 ±0.009	2.827 ±0.009
54007.9556	15.259 ±0.012	1.182 ±0.020	2.171 ±0.017	2.787 ±0.019
54009.9578	15.252 ±0.010	1.176 ±0.021	2.171 ±0.022	2.776 ±0.022
54010.9527	15.196 ±0.030	1.234 ±0.035	2.100 ±0.047	2.785 ±0.038
54011.9523	15.239 ±0.015	1.233 ±0.025	2.161 ±0.027	2.750 ±0.034
54012.9470	15.234 ±0.015	1.234 ±0.041	2.111 ±0.032	2.806 ±0.034
54015.9420	15.235 ±0.010	1.202 ±0.028	2.137 ±0.015	2.796 ±0.017
54016.9380	15.218 ±0.008	1.050 ±0.026	2.127 ±0.009	2.797 ±0.010
54018.9322	15.221 ±0.008	1.134 ±0.024	2.145 ±0.011	2.795 ±0.015
54034.9093	15.206 ±0.009	0.895 ±0.043	2.114 ±0.009	2.778 ±0.008
54062.8373	15.562 ±0.014	1.336 ±0.034	2.409 ±0.019	2.899 ±0.018
54088.7768	15.733 ±0.016	1.600 ±0.076	2.558 ±0.018	2.909 ±0.013
54089.7971	15.786 ±0.012	1.837 ±0.047	2.595 ±0.014	2.910 ±0.011
54090.7216	15.771 ±0.012	1.756 ±0.044	2.613 ±0.015	2.898 ±0.012
54090.7773	15.771 ±0.009	1.806 ±0.031	2.580 ±0.011	2.905 ±0.013
54090.8348	15.764 ±0.014	1.804 ±0.033	2.551 ±0.020	2.943 ±0.020
54090.8953	15.772 ±0.014	1.753 ±0.038	2.615 ±0.024	2.888 ±0.023
54091.8777	15.745 ±0.015	1.511 ±0.056	2.578 ±0.016	2.900 ±0.012
54093.8949	15.701 ±0.012	1.618 ±0.043	2.515 ±0.017	2.892 ±0.014
54094.8819	15.704 ±0.008	1.679 ±0.035	2.525 ±0.010	2.882 ±0.010
54095.8869	15.740 ±0.010	1.709 ±0.030	2.541 ±0.020	2.892 ±0.021
54096.7148	15.709 ±0.011	1.721 ±0.025	2.564 ±0.016	2.807 ±0.014
54101.6974	15.543 ±0.011	1.536 ±0.036	2.413 ±0.012	2.799 ±0.011
54102.6882	15.571 ±0.011	1.444 ±0.045	2.460 ±0.015	2.784 ±0.016
54103.6947	15.502 ±0.014	1.406 ±0.044	2.391 ±0.014	2.769 ±0.008
54104.6990	15.381 ±0.009	1.311 ±0.039	2.259 ±0.012	2.658 ±0.010
54105.8278	15.305 ±0.009	1.196 ±0.023	2.223 ±0.014	2.700 ±0.013
54107.6969	15.351 ±0.010	1.307 ±0.024	2.268 ±0.011	2.730 ±0.013
54108.8268	15.312 ±0.009	1.221 ±0.022	2.312 ±0.011	2.748 ±0.009
54109.6713	15.244 ±0.010	1.227 ±0.028	2.183 ±0.013	2.721 ±0.011
54110.6660	15.235 ±0.009	1.247 ±0.020	2.181 ±0.010	2.700 ±0.008
54112.7732	15.164 ±0.009	1.231 ±0.015	2.118 ±0.015	2.670 ±0.015
54115.8588	15.186 ±0.009	1.211 ±0.017	2.095 ±0.014	2.723 ±0.014
54116.8586	15.180 ±0.006	1.201 ±0.018	2.125 ±0.008	2.622 ±0.009
54117.8579	15.178 ±0.010	1.221 ±0.017	2.119 ±0.011	2.703 ±0.012
54121.6675	15.252 ±0.016	1.461 ±0.038	2.200 ±0.026	2.679 ±0.026
54124.6630	15.229 ±0.014	1.214 ±0.018	2.106 ±0.018	2.727 ±0.015
54125.6276	15.160 ±0.010	1.158 ±0.022	2.137 ±0.011	2.677 ±0.008
54126.6314	15.178 ±0.011	1.240 ±0.020	2.161 ±0.014	2.637 ±0.013
54127.8740	15.172 ±0.010	1.210 ±0.021	2.165 ±0.011	2.664 ±0.008
54128.6324	15.161 ±0.009	1.195 ±0.019	2.129 ±0.014	2.683 ±0.014
54135.7395	15.091 ±0.008	1.145 ±0.018	2.082 ±0.010	2.637 ±0.011
54137.8268	15.103 ±0.009	1.208 ±0.019	2.082 ±0.011	2.636 ±0.010
54139.6145	15.112 ±0.009	1.166 ±0.018	2.101 ±0.013	2.642 ±0.012
54141.6137	15.128 ±0.011	1.208 ±0.023	2.071 ±0.015	2.665 ±0.015
54144.6157	15.135 ±0.011	1.196 ±0.016	2.129 ±0.014	2.638 ±0.018
54145.6680	15.162 ±0.016	1.223 ±0.027	2.135 ±0.017	2.674 ±0.012
54146.6189	15.181 ±0.012	1.257 ±0.020	2.170 ±0.017	2.659 ±0.017
54148.6148	15.185 ±0.009	1.256 ±0.017	2.156 ±0.015	2.649 ±0.017
54149.6236	15.168 ±0.007	1.244 ±0.014	2.149 ±0.010	2.645 ±0.010
54150.6415	15.147 ±0.030	1.250 ±0.033	2.128 ±0.035	2.651 ±0.022
54153.6224	15.176 ±0.012	1.230 ±0.020	2.158 ±0.016	2.652 ±0.012
54155.6250	15.098 ±0.008	1.202 ±0.015	2.089 ±0.010	2.634 ±0.010
54158.7223	15.198 ±0.010	1.274 ±0.017	2.181 ±0.011	2.504 ±0.018
54160.6141	15.187 ±0.010	1.203 ±0.027	2.169 ±0.010	2.661 ±0.006
54161.6427	15.181 ±0.009	1.233 ±0.020	2.147 ±0.011	2.664 ±0.011
54166.6151	15.156 ±0.012	1.264 ±0.018	2.153 ±0.016	2.611 ±0.014
54168.6155	15.187 ±0.008	1.261 ±0.017	2.146 ±0.012	2.642 ±0.012
54175.6270	15.177 ±0.010	1.224 ±0.026	2.157 ±0.011	2.664 ±0.011
54186.6278	15.268 ±0.020	1.360 ±0.037	2.270 ±0.024	2.688 ±0.026
54195.6474	15.136 ±0.011	1.345 ±0.032	2.130 ±0.017	2.631 ±0.026

Table 3. Identification of emission lines in the WHT + ISIS spectra of V838 Mon for December 18 (4724 ≤ λ ≤ 5544 Å) and December 26 (λ ≤ 4723 and λ ≥ 5862 Å). The integrated line fluxes are given both in units of erg cm^{-2} s^{-1} as well as relative to Hβ. The wavelengths are heliocentric and the fluxes are not corrected for reddening.

$\lambda_\odot^{obs}$ (Å)	Flux	$\frac{F_\lambda}{F_{H\beta}}$	E.W. (Å)	ident	$\lambda_\odot^{obs}$ (Å)	Flux	$\frac{F_\lambda}{F_{H\beta}}$	E.W. (Å)	ident	$\lambda_\odot^{obs}$ (Å)	Flux	$\frac{F_\lambda}{F_{H\beta}}$	E.W. (Å)	ident
3914.168	1.955E-16	0.091	0.881		4369.255	1.468e-16	0.069	0.414	FeII 28	4950.899	1.166e-15	0.546	0.761	[FeII] 20
3915.746	9.701E-17	0.045	0.430		4372.325	1.289e-15	0.603	3.484	[FeII] 21	4957.567	9.136e-17	0.043	0.277	[FeII] 4
3938.876	2.420E-16	0.113	0.999		4382.591	5.544e-16	0.259	1.550	[FeII] 6	4973.627	1.947e-15	0.911	6.099	[FeII] 20
3945.643	1.670E-16	0.078	0.762		4384.093	3.027e-16	0.142	0.850	[FeII] 36	4997.287	6.301e-16	0.295	1.071	
3969.901	2.490E-16	0.117	1.514	Hε	4385.217	6.392e-16	0.299	1.802	FeII 27	5005.792	2.887e-16	0.135	0.688	[FeII] 20
3974.662	2.476E-16	0.116	1.407		4399.782	1.433e-16	0.067	0.259	FeII 20	5007.007	6.896e-16	0.323	1.591	[Fe II] 4
3993.008	9.988e-16	0.467	3.779	[Ni II] 4	4402.687	4.885e-17	0.023	0.131	[FeII] 36	5018.640	6.799e-15	3.182	13.70	FeII 42
4017.244	7.673e-17	0.036	0.312	[Fe II] 24	4413.662	4.618e-15	2.161	13.68	[FeII] 7	5020.470	1.976e-15	0.925	3.967	[FeII] 20
4032.927	3.378e-16	0.158	1.499	[Ni II] 4	4416.195	4.832e-15	2.261	15.47	[FeII] 6	5035.589	9.209e-17	0.043	0.084	[FeII] 4
4033.719	1.021e-16	0.048	0.456	[Fe II] 24	4432.343	3.592e-16	0.168	1.413	[FeII] 6	5043.886	1.399e-15	0.655	1.366	[FeII] 20
4066.897	1.856e-16	0.087	0.669	NiII 11	4439.661	5.947e-17	0.028	0.219	[FeII] 36	5048.337	1.098e-15	0.514	1.213	[FeII]
4068.350	1.165e-15	0.545	4.199	[SII] 1	4451.988	3.096e-15	1.449	7.827	[FeII] 7	5071.859	4.012e-16	0.188	0.255	[Fe II] 19
4076.368	1.936e-16	0.091	0.730	[SII] 1	4457.859	2.658e-15	1.244	7.050	[FeII] 6	5083.447	5.097e-16	0.239	0.5085	[Fe II] 35
4079.870	8.076e-17	0.038	0.286	[Fe II] 24	4461.023	5.772e-17	0.027	0.169	[Ni II] 10	5107.697	9.084e-16	0.425	0.733	[Fe II] 18
4084.290	4.009e-17	0.019	0.166	[Fe II] 24	4470.143	1.157e-16	0.054	0.482	[FeII] 6	5112.083	1.244e-15	0.582	0.820	[Fe II] 19
4097.349	2.196e-16	0.103	0.881		4472.726	1.605e-16	0.075	0.595	FeII 37	5158.792	1.348e-14	6.308	8.426	e
4101.669	1.274e-16	0.060	0.610	Hδ	4474.787	1.355e-15	0.634	4.585	[FeII] 7	5163.993	3.669e-15	1.717	3.814	[FeII] 35
4102.885	9.526e-17	0.045	0.471		4478.958	1.305e-16	0.061	0.432	[Fe II]	5169.236	7.032e-15	3.291	14.08	FeII 42
4114.397	5.982e-16	0.280	2.093	[FeII] 23	4485.133	3.404e-16	0.159	0.907	[NiII] 3	5182.010	1.690e-15	0.791	3.849	[FeII] 18
4122.504	2.503e-16	0.117	0.913	FeII 28	4488.785	1.670e-15	0.781	4.063	d	5197.798	4.702e-15	2.200	7.769	FeII 49
4124.741	6.971e-17	0.033	0.253	FeII 22	4491.230	9.509e-16	0.445	2.410	FeII 37	5199.490	2.243e-15	1.050	3.604	[FeII] 35
4128.286	9.345e-17	0.044	0.328	FeII 27	4492.508	7.620e-16	0.357	2.078	[FeII] 6	5220.175	2.063e-15	0.965	1.722	[FeII] 19
4144.038	2.010e-16	0.094	0.718	FeII 45	4508.090	8.930e-16	0.418	2.684	FeII 38	5234.710	3.698e-15	1.730	6.277	FeII 49
4145.810	4.687e-17	0.022	0.169	[Fe II] 21	4509.476	3.799e-16	0.178	1.132	[FeII] 6	5261.764	6.929e-15	3.242	5.186	[FeII] 19
4147.130	1.946e-16	0.091	0.700	[Ni II] 10	4515.090	2.044e-15	0.956	5.751	FeII 37	5268.990	2.890e-15	1.352	2.358	[FeII] 18
4152.612	3.787e-16	0.177	1.178		4520.070	1.440e-15	0.674	4.343	FeII 37	5273.560	8.646e-15	4.046	6.392	[FeII] 18
4173.296	6.579e-16	0.308	2.285	FeII 27	4522.458	1.113e-15	0.521	3.225	FeII 38	5276.062	4.482e-15	2.097	3.344	FeII 49
4177.177	1.015e-15	0.475	3.562	[FeII] 21	4528.277	3.580e-16	0.168	0.949	[FeII] 6	5284.133	2.233e-15	1.045	1.907	FeII 41
4178.730	1.591e-15	0.745	5.632	FeII 28	4532.806	1.602e-16	0.075	0.423	[FeII] 6	5296.950	9.714e-16	0.455	0.697	[FeII] 19
4201.154	8.327e-16	0.390	2.466	[Ni II] 3	4533.953	3.511e-16	0.164	0.930	FeII 37	5316.708	1.175e-14	5.498	8.765	FeII 49
4205.278	3.713e-17	0.017	0.131	FeII 22	4541.415	3.805e-16	0.178	1.022	FeII 38	5325.739	6.505e-16	0.304	0.380	FeII 49
4211.006	2.795e-16	0.131	0.901	[FeII]	4547.451	1.873e-16	0.088	0.665		5333.787	6.369e-15	2.980	3.845	[FeII] 19
4231.896	5.303e-16	0.248	1.915	[FeII] 21	4549.318	1.906e-15	0.892	6.735	FeII 38	5347.367	1.383e-15	0.647	0.969	f
4233.065	2.458e-15	1.150	8.106	FeII 27	4555.725	2.036e-15	0.953	5.172	FeII 37	5362.948	1.845e-15	0.863	1.511	FeII 48
4244.033	6.187e-15	2.895	17.97	[FeII] 21	4558.462	1.205e-16	0.056	0.296	FeII 20	5376.509	5.346e-15	2.502	2.909	[FeII] 19
4248.812	4.465e-16	0.209	1.354	[Ni II] 4	4571.931	1.938e-16	0.091	0.408		5412.494	3.882e-15	1.817	2.077	[FeII] 17
4251.324	1.966e-16	0.092	0.676	[FeII]	4576.210	6.520e-16	0.305	1.649	FeII 38	5425.251	6.248e-16	0.292	0.204	FeII 49
4258.069	2.512e-16	0.118	0.806	FeII 28	4577.707	3.843e-17	0.018	0.101	FeII 54	5433.327	2.930e-15	1.371	1.584	[FeII] 18
4266.264	5.328e-17	0.025	0.161	[FeII] 36	4582.638	4.620e-16	0.216	1.374	FeII 37	5477.219	1.572e-15	0.736	2.763	FeII 49
4273.142	1.079e-16	0.050	0.388	FeII 27	4583.669	2.811e-15	1.315	8.397	FeII 38	5495.648	2.386e-15	1.117	2.337	[FeII] 17
4276.742	3.525e-15	1.650	11.97	[FeII] 21	4587.988	7.871e-17	0.037	0.280		5527.233	5.134e-15	2.402	2.532	[FeII] 17
4277.790	3.012e-16	0.141	0.942	FeII 32	4595.896	8.713e-17	0.041	0.327	FeII 38	5869.959	6.091e-16	0.285	1.268	[Fe II]
4285.018	8.620e-18	0.004	0.021	[Ni II] 4	4620.318	2.259e-16	0.106	0.506	FeII 38	5884.880	1.536e-16	0.072	0.369	Fe II
4287.286	8.386e-15	3.924	25.78	[FeII] 7	4627.870	2.895e-16	0.135	0.897	FeII 54	5901.304	3.687e-16	0.173	0.797	[FeII] 34
4290.240	5.822e-17	0.027	0.180	TiII 41	4627.972	2.923e-16	0.137	0.956	[Ni II] 3	5902.591	2.893e-16	0.135	0.646	FeII
4293.999	4.498e-16	0.210	1.410	[Ni II] 4	4629.167	2.974e-15	1.392	9.045	FeII 37	5991.293	2.100e-16	0.098	0.080	FeII
4296.392	5.811e-16	0.272	1.792	FeII 28	4639.562	1.311e-15	0.613	3.893	[FeII] 4	6044.056	4.384e-16	0.205	0.468	[Fe II]
4299.944	1.186e-16	0.055	0.362	TiII 41	4656.823	1.241e-16	0.058	0.445	FeII 43	6147.661	2.002e-16	0.094	0.237	FeII 74
4303.001	5.733e-16	0.268	1.701	FeII 27	4657.796	9.865e-17	0.046	0.350		6149.160	2.995e-16	0.140	0.505	FeII 74
4305.789	1.073e-15	0.502	3.179	[FeII] 21	4664.248	5.509e-16	0.258	1.680	a	6158.064	4.301e-16	0.201	1.073	Fe II
4307.862	7.637e-17	0.036	0.276	TiII 41	4666.613	6.000e-16	0.281	1.817	FeII 37	6160.959	1.671e-16	0.078	0.441	Fe II
4310.063	3.499e-17	0.016	0.118	[Ni II] 10	4670.032	1.298e-16	0.061	0.454		6172.577	1.978e-16	0.093	0.524	Fe II
4312.643	3.944e-17	0.018	0.114	TiII 41	4672.389	1.068E-16	0.050	0.100	[Ni II] 10	6233.435	4.697e-16	0.220	0.822	FeII
4314.131	2.570e-16	0.120	0.759	FeII 32	4728.271	3.873e-15	1.812	7.105	[FeII] 4	6238.295	5.953e-16	0.279	0.773	FeII 74
4314.797	2.734e-17	0.013	0.082	TiII 41	4731.573	4.278e-16	0.200	0.717	FeII 43	6239.742	1.569e-16	0.073	0.186	FeII 74
4319.530	2.422e-15	1.133	7.153	[FeII] 21	4772.124	2.987e-16	0.140	0.993	[FeII] 4	6247.441	1.278e-15	0.598	0.887	FeII 74
4326.189	7.842e-16	0.367	2.348	[Ni II] 3	4774.911	1.889e-16	0.088	0.884	[FeII] 20	6248.792	1.170e-15	0.547	0.741	Fe II
4326.990	3.656e-17	0.017	0.111	FeII 20	4798.504	6.191e-16	0.290	1.152	b	6300.224	1.445e-14	6.762	10.16	[OI] 1
4328.883	5.194e-17	0.024	0.164		4802.822	7.431e-16	0.348	1.597		6317.851	2.519e-15	1.179	0.580	Fe II
4329.350	3.365e-17	0.016	0.106	[FeII] 36	4814.759	6.370e-15	2.981	16.61	[FeII] 20	6363.668	4.714e-15	2.206	4.166	[OI] 1
4338.403	4.900e-17	0.023	0.232	FeII 32	4853.046	1.968e-16	0.092	0.565	[FeII] 20	6383.585	1.970e-15	0.922	0.399	Fe II
4340.426	2.996e-16	0.140	1.210	Hγ	4861.522	2.137e-15	1.000	7.865	Hβ	6416.845	5.071e-16	0.237	0.119	FeII 74
4346.732	1.025e-15	0.480	4.051	[FeII] 21	4874.756	2.205e-15	1.032	5.183	[FeII] 20	6456.200	3.936e-15	1.842	0.633	FeII 74
4351.815	1.322e-15	0.619	4.524	FeII 27	4889.837	5.372e-15	2.514	8.231	[FeII] 4	6491.115	7.263e-16	0.340	0.119	Fe II
4352.670	1.646e-15	0.770	5.576	[FeII] 21	4898.803	1.494e-15	0.699	2.119	[Fe II]	6492.932	9.711e-16	0.454	0.155	Fe II
4358.166	2.363e-15	1.106	6.741	c	4905.579	3.385e-15	1.584	4.127	[FeII] 20	6516.938	9.349e-16	0.437	0.123	Fe II
4359.213	6.515e-15	3.049	18.58	[FeII] 7	4924.170	6.343e-15	2.968	6.413	FeII 42	6562.940	2.234e-13	104.5	24.69	Hα
4364.722	1.406e-16	0.066	0.389		4947.622	8.234e-16	0.385	0.562	[FeII] 20	6586.655	8.059e-16	0.377	0.104	Fe II

a: blend of [FeII] 4 4664.440 and [FeII]4 4665.645 Å
b: blend of [FeII] 4 4798.274 and [FeII] 4 4799.293 Å
c: blend of [FeII] 6 4358.095 and [Fe II] 21 4358.471 Å
d: blend of [FeII] 6 4488.749 and Fe II 37 4489.183 Å
e: blend of [FeII] 18 5158.001 and [Fe II] 19 5158.777 Å
f: blend of [FeII] 18 5347.653 and Fe II 49 5347.228 Å

Table 4. The emission lines in Table 3 are arranged in multiplets and their intensity – this time corrected for $E_{B-V} = 0.87$ reddening (Munari et al. 2005) – is given relative to the strongest line of each multiplet. The wavelengths are corresponding laboratory ones.

λ_{lab} (Å)	dered F_λ/F_λ^P	E.W. (Å)	multiplet	λ_{lab} (Å)	dered. F_λ/F_λ^P	E.W. (Å)	multiplet	λ_{lab} (Å)	dered. F_λ/F_λ^P	E.W. (Å)	multiplet
4639.666	0.342	3.893	[FeII] 4	4146.649	0.008	0.169	[FeII] 21	4508.283	0.318	2.684	FeII 38
4665.043	0.144	1.680	[FeII] 4[a]	4177.196	0.164	3.562	[FeII] 21	4522.634	0.396	3.225	FeII 38
4728.068	0.721	7.105	[FeII] 4	4231.554	0.086	1.915	[FeII] 21	4541.523	0.135	1.022	FeII 38
4772.062	0.035	0.993	[FeII] 4	4244.143	1.000	17.97	[FeII] 21	4549.467	0.678	6.735	FeII 38
4798.783	0.115	1.152	[FeII] 4[b]	4276.829	0.570	11.97	[FeII] 21	4576.331	0.232	1.649	FeII 38
4889.617	1.000	8.231	[FeII] 4	4305.890	0.173	3.179	[FeII] 21	4583.829	1.000	8.397	FeII 38
4957.914	0.011	0.277	[FeII] 4	4319.619	0.391	7.153	[FeII] 21	4596.218	0.031	0.327	FeII 38
5006.624	0.081	1.591	[FeII] 4	4346.852	0.166	4.051	[FeII] 21	4620.513	0.080	0.506	FeII 38
5035.484	0.011	0.084	[FeII] 4	4352.778	0.266	5.576	[FeII] 21				
				4358.471	0.191	3.341	[FeII] 21[h]	4923.921	0.902	6.413	FeII 42
4358.095	0.244	3.341	[FeII] 6[c]	4372.427	0.208	3.484	[FeII] 21	5018.434	0.967	13.70	FeII 42
4382.742	0.115	1.550	[FeII] 6					5169.030	1.000	14.08	FeII 42
4416.266	1.000	15.47	[FeII] 6	4017.378	0.751	0.312	[FeII] 24				
4432.447	0.074	1.413	[FeII] 6	4033.972	1.000	0.456	[FeII] 24	4656.974	0.407	0.445	FeII 43
4457.945	0.550	7.050	[FeII] 6	4079.989	0.791	0.286	[FeII] 24	4731.439	1.000	0.717	FeII 43
4470.294	0.024	0.482	[FeII] 6	4084.320	0.393	0.166	[FeII] 24				
4488.749	0.176	2.063	[FeII] 6[d]					5197.888	0.418	8.748	FeII 49
4492.634	0.158	2.078	[FeII] 6	5083.731	0.088	0.5085	[FeII] 35	5234.620	0.315	6.277	FeII 49
4509.602	0.079	1.132	[FeII] 6	5163.951	1.000	3.814	[FeII] 35	5275.994	0.381	3.344	FeII 49
4528.384	0.074	0.949	[FeII] 6	5199.173	0.385	3.604	[FeII] 35	5316.609	1.000	8.765	FeII 49
4533.003	0.033	0.423	[FeII] 6					5325.553	0.035	0.380	FeII 49
				4266.349	0.176	0.161	[FeII] 36	5347.228	0.118	0.969	FeII 49
4287.394	1.000	25.78	[FeII] 7	4329.430	0.111	0.106	[FeII] 36	5425.257	0.034	0.204	FeII 49
4359.333	0.777	18.58	[FeII] 7	4384.210	1.000	0.850	[FeII] 36	5476.989	0.134	2.763	FeII 49
4413.781	0.551	13.68	[FeII] 7	4402.560	0.161	0.131	[FeII] 36				
4452.098	0.369	7.827	[FeII] 7	4439.710	0.196	0.219	[FeII] 36	4577.791	0.133	0.101	FeII 54
4474.904	0.162	4.585	[FeII] 7					4627.866	1.000	0.897	FeII 54
				4327.039	0.255	0.111	FeII 20				
5412.654	0.756	2.077	[FeII] 17	4399.858	1.000	0.259	FeII 20	6147.735	0.051	0.237	FeII 74
5495.824	0.465	2.337	[FeII] 17	4558.572	0.840	0.296	FeII 20	6149.238	0.076	0.505	FeII 74
5527.339	1.000	2.532	[FeII] 17					6238.375	0.151	0.773	FeII 74
				4124.793	1.000	0.253	FeII 22	6239.953	0.040	0.186	FeII 74
5107.942	0.066	0.733	[FeII] 18	4205.473	0.533	0.131	FeII 22	6247.562	0.325	0.887	FeII 74
5158.001	0.491	4.213	[FeII] 18[e]					6416.905	0.129	0.119	FeII 74
5181.948	0.195	3.849	[FeII] 18	4128.735	0.038	0.328	FeII 27	6456.376	1.000	0.633	FeII 74
5268.875	0.334	2.358	[FeII] 18	4173.450	0.268	2.285	FeII 27				
5273.346	1.000	6.392	[FeII] 18	4233.167	1.000	8.106	FeII 27	6300.304	1.000	10.16	[OI] 1
5347.653	0.050	0.485	[FeII] 18[f]	4273.317	0.044	0.388	FeII 27	6363.777	0.326	4.166	[OI] 1
5433.129	0.339	1.584	[FeII] 18	4303.166	0.233	1.701	FeII 27				
				4351.764	0.538	4.524	FeII 27	4068.600	1.000	4.199	[SII] 1
5072.392	0.037	0.255	[FeII] 19	4385.381	0.260	1.802	FeII 27	4076.349	0.166	0.730	[SII] 1
5111.627	0.113	0.820	[FeII] 19								
5158.777	0.613	4.213	[FeII] 19[g]	4122.638	0.157	0.913	FeII 28	4290.222	0.491	0.180	TiII 41
5220.059	0.298	1.722	[FeII] 19	4178.855	1.000	5.632	FeII 28	4300.052	1.000	0.362	TiII 41
5261.621	1.000	5.186	[FeII] 19	4258.155	0.158	0.806	FeII 28	4307.900	0.644	0.276	TiII 41
5296.829	0.140	0.697	[FeII] 19	4296.567	0.365	1.792	FeII 28	4312.861	0.333	0.114	TiII 41
5333.646	0.919	3.845	[FeII] 19	4369.404	0.092	0.414	FeII 28	4314.979	0.231	0.082	TiII 41
5376.452	0.771	2.909	[FeII] 19								
				4278.13	1.000	0.942	FeII 32	4201.171	1.000	2.466	[NiII] 3
4774.718	0.296	6.730	[FeII] 20	4314.29	0.853	0.759	FeII 32	4326.236	0.942	2.348	[NiII] 3
4814.534	1.000	16.61	[FeII] 20	4338.70	0.163	0.232	FeII 32	4485.212	0.401	0.879	[NiII] 3
4852.730	0.019	0.565	[FeII] 20					4628.046	0.351	0.956	[NiII] 3
4874.485	0.346	5.183	[FeII] 20	4472.921	0.054	0.595	FeII 37				
4905.339	0.531	4.127	[FeII] 20	4489.185	0.286	2.063	FeII 37[i]	3993.059	1.000	3.779	[NiII] 4
4947.373	0.129	0.562	[FeII] 20	4491.401	0.320	2.410	FeII 37	4033.038	0.423	1.782	[NiII] 4
4950.744	0.183	0.761	[FeII] 20	4515.337	0.687	5.751	FeII 37	4248.799	0.447	1.354	[NiII] 4
4973.388	0.306	6.099	[FeII] 20	4520.225	0.484	4.343	FeII 37	4285.306	0.009	0.021	[NiII] 4
5005.512	0.386	6.703	[FeII] 20	4534.166	0.118	0.930	FeII 37	4294.092	0.450	1.410	[NiII] 4
5020.233	0.310	3.967	[FeII] 20	4555.890	0.685	5.172	FeII 37				
5043.520	0.220	1.366	[FeII] 20	4582.835	0.155	1.374	FeII 37	4147.238	1.000	0.700	[NiII] 10
				4629.336	1.000	9.045	FeII 37	4310.341	0.180	0.118	[NiII] 10
				4666.750	0.202	1.817	FeII 37	4461.464	0.780	0.441	[NiII] 10
								4573.357	0.247	0.100	[NiII] 10

a: blend of 4664.440, 4665.645 Å lines of this same multiplet
b: blend of 4798.274, 4799.293 Å lines of this same multiplet
c: unresolved blend with [Fe II] 21 4358.471. Flux split half-and-half between the two lines.
d: unresolved blend with Fe II 37 4489.183. Flux split half-and-half between the two lines.
e: unresolved blend with [Fe II] 19 5158.777. Flux split half-and-half between the two lines.
f: unresolved blend with Fe II 49 5347.228. Flux split half-and-half between the two lines.
g: unresolved blend with [Fe II] 18 5158.001. Flux split half-and-half between the two lines.
h: unresolved blend with [FeII] 6 4358.095. Flux split half-and-half between the two lines.
i: unresolved blend with [FeII] 6 4488.749. Flux split half-and-half between the two lines.